NANO LETTERS
Letter
Cite This: Nano Lett. 2019, 19, 5769−5773
pubs.acs.org/NanoLett

Dynamical Metal to Charge-Density-Wave Junctions in an Atomic Wire Array

Sun Kyu Song,[†,‡] Abdus Samad,[¶] Stefan Wippermann,[¶] and Han Woong Yeom*[,†,‡]

[†]Center for Artificial Low Dimensional Electronic Systems, Institute for Basic Science (IBS), Pohang 37673, Republic of Korea
[‡]Department of Physics, Pohang University of Science and Technology (POSTECH), Pohang 37673, Republic of Korea
[¶]Max-Planck-Institut für Eisenforschung GmbH, Düsseldorf 40237, Germany

Supporting Information

ABSTRACT: We investigated the atomic scale electronic phase separation emerging from a quasi-1D charge-density-wave (CDW) state of the In atomic wire array on a Si(111) surface. Spatial variations of the CDW gap and amplitude are quantified for various interfaces of metallic and insulating CDW domains by scanning tunneling microscopy and spectroscopy (STS). The strong anisotropy in the metal−insulator junctions is revealed with an order of magnitude difference in the interwire and intrawire junction lengths of 0.4 and 7 nm, respectively. The intrawire junction length is reduced dramatically by an atomic scale impurity, indicating the tunability of the metal−insulator junction in an atomic scale. Density functional theory calculations disclose the dynamical nature of the intrawire junction formation and tunability.

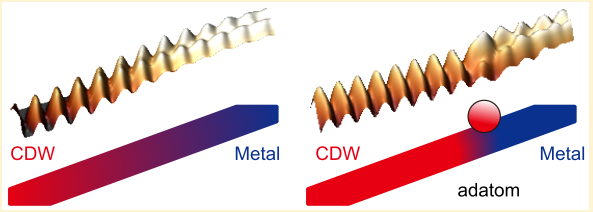

KEYWORDS: *Atomic wire, charge-density-wave, electronic phase separation, metal−insulator junction, scanning tunneling microscopy/spectroscopy*

Electronic phase separation (EPS), the coexistence of different electronic or magnetic phases at low temperatures,[1] is an intriguing phenomenon related to exotic electronic systems such as colossal magnetoresistance[2] and high-temperature superconductivity.[3,4] Beyond fascinating fundamental questions, EPS may provide an extra control knob on the functionality based on those competing states. Since the coexistence of different phases occurs in length scales of from a few nanometers[5] to micrometers,[2,6,7] a microscopic investigation in real space is essential to understand the underlying physics and the functionality. However, although several previous studies performed microscopic measurements on EPS phenomena,[2,3,5−9] very few could access interfaces or junctions between distinct electronic phases at an atomic scale. At large, the microscopic properties of those interfaces are unknown.[8,9]

In recent studies,[10,11] EPS between a metallic and a manybody insulating phase of the charge-density-wave (CDW) has been reported in the quasi-1D indium atomic wire array on a Si(111) surface and in various quasi-2D layered chalcogenide systems.[12−14] In the latter systems, EPS has been actively discussed together with complex interactions for emerging superconductivity,[15] hidden order,[16] and novel functionalities such as ultrafast resistive switching,[17,18] oscillators,[19] and memristors.[20] On the other hand, the In atomic wire array on Si(111) provides a unique platform to investigate EPS in a quasi-1D system and a stepping stone toward understanding more complex quasi-2D cases. This system features a CDW phase transition between the metallic 4 × 1 phase and the insulating 8 × 2 phase at ∼125 K.[21] Both phases could be stabilized well below the transition temperature (T_C) by controlling the density of defects, such as vacancies and adsorbates.[10,11] Considering the fact that a pure CDW insulator is rare in 2D systems due to various other manybody interactions involved, a well-defined CDW insulating state in this system provides an important aspect as a model system for the investigation of the EPS and interfaces with CDW. The other merits of this system are a sufficiently high CDW transition temperature and the easy accessibility for atomic scale probes.

In this Letter, we utilize the In/Si(111) system to understand how electronic junctions for EPS are formed in an atomic scale. Using scanning tunneling microscopy/spectroscopy (STM/STS), we examine atomic scale spatial variations of the CDW amplitude/gap and the local lattice distortion crossing different types of phase boundaries between metallic and CDW phases. We observe a pronounced anisotropy in the electronic junction lengths of interwire and intrawire phase boundaries. We clearly distinguish intrinsic and extrinsic, impurity-induced, junctions; the electronic junction length can be reduced drastically by a specific impurity. First-principles calculations reveal a dynamical mechanism of the electronic junction formation and its pinning by such an impurity. These results provide an important insight toward

Received: June 15, 2019
Revised: July 3, 2019
Published: July 5, 2019

DOI: 10.1021/acs.nanolett.9b02438
Nano Lett. 2019, 19, 5769−5773

the control over electronic interfaces and phase separations in complex materials.

Our experiments were performed in a commercial ultrahigh vacuum cryogenic STM (SPECS, Germany). The Si(111)4 × 1-In surface (Figure S1 in Supporting Information) was prepared by thermally depositing In atoms of ∼1 monolayer (ML) onto the clean Si(111) 7 × 7 surface kept at 600 K.[21] The STS spectra, dI/dV curves of the tunneling current, were obtained using the lock-in technique. Most of the experimental data were acquired at 78 K, which is well below T_C. Density functional theory (DFT) calculations were performed using the VASP package[22] with numerical details as described before.[23]

Figure 1a shows the electronically phase-separated In atomic wire array on a Si(111) surface taken at 78 K, well below its T_C. Brighter regions exhibit rows of protrusions corresponding to a_0 (the lattice constant of the substrate surface, 0.384 nm) periodicity of the metallic 4 × 1 phase (Figure 1b).[24] Within regions of darker contrast, rows of oval-shaped protrusions with a $2a_0$ periodicity are observed, which correspond to the insulating CDW (8 × 2) phase (Figure 1b).[25] The coexistence of two distinct electronic phases is apparent from the inhomogeneous mixture of bright and dark STM contrast, which is due to metallic electrons being present only in the 4 × 1 phase. In previous studies, the phase coexistence and the decrease of T_C was induced by introducing extrinsic defects such as Na, oxygen or In adsorbates, and vacancies.[10,11,26,27] It was suggested that the phase coexistence originates from electron doping[10] or local strain.[11] In the present study, the EPS can be accessed in samples with unoptimized In coverages and can be systematically controlled by extra In deposition. Figure 1a also shows defects in the forms of dark vacancy clusters, bright adatom clusters, and atomic scale defects. Clusters of vacancies and adatoms (within boxes) have ill defined irregular structures, but there also exist various types of atomic scale defects with better defined structures and a much higher population (within circles). Hereafter, we put aside the issue of the underlying mechanism of EPS and focus on electronic interfaces formed as its consequence as well as the effects of well-defined atomic scale defects.

Metal−insulator junctions are formed both parallel and perpendicular to the atomic wires. Note the strong anisotropy of the junctions reflecting obviously the quasi-1D nature of the In atomic wire array; long and straight along the wires but short and irregular in the perpendicular direction. Figure 1b shows a detailed STM image of a representative intrawire metal−insulator junction located far from any defects. The STM topography shows clearly the change of the atomic structure across this intrinsic interface. At the left-hand side, the oval-shaped protrusions of In hexagon chains in the 8 × 2 phase are observed. At the opposite side, two rows of protrusions with a_0 periodicity appear, representing the double In zigzag chain structure of the 4 × 1 phase. In between, the ×2 structural distortion of the 8 × 2 phase or the CDW amplitude decays gradually over a distance of 7 nm as quantitatively plotted in Figure 1d (green dots).

In a CDW system, the change of the atomic structure between two phases would be entangled with the electronic structure as shown in the dI/dV map (Figure 1c). The typical STS spectrum of the 8 × 2 structure (the black curve) in the inset of Figure 1d clearly shows the CDW gap near the Fermi level. The gap size is about 250 meV when estimated from the spectral range with null conductance between −170 and 80

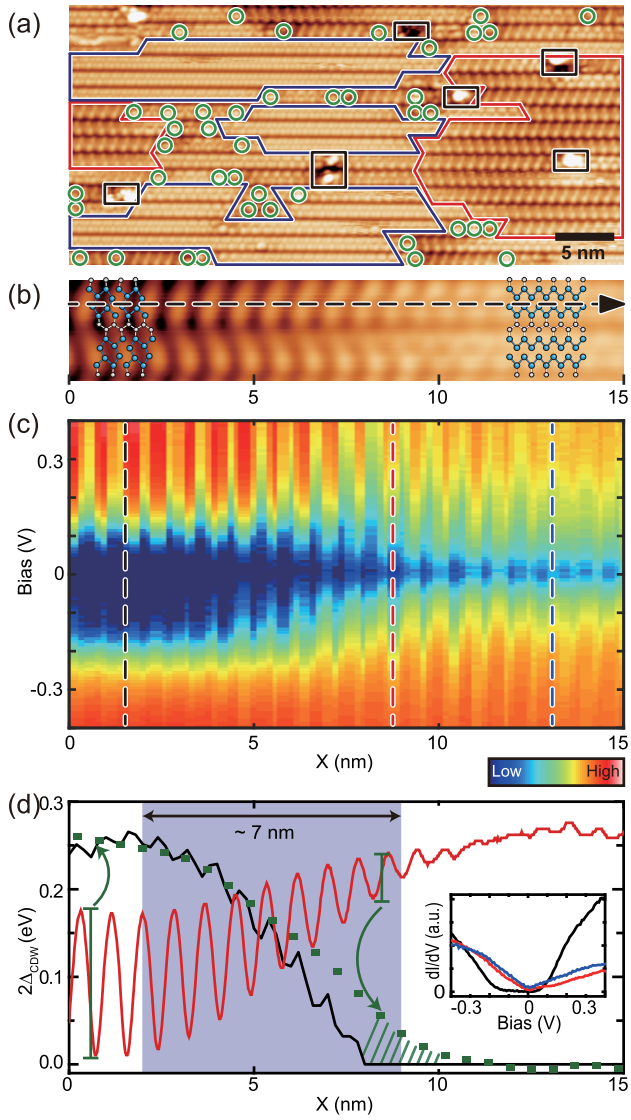

Figure 1. (a) STM image of the electronic phase-separated state taken at V_s = −0.5 V and I_t = 100 pA. The bright regions (blue boxes) indicate the 4 × 1 phase, and the dark regions (red boxes) indicate the 8 × 2 phase. Typical defects are marked as black boxes. (b) STM image of the intrawire junction between 8 × 2 and 4 × 1 phases taken at V_s = −0.5 V and I_t = 100 pA. (c) The spatially resolved dI/dV map (plotted in a logarithmic scale) of the intrawire junction taken along the black arrow in panel b. The vertical dashed lines indicate the position where the dI/dV curves in the inset of panel d are obtained. (d) The spatial distributions of the CDW gap (the black curve) and the CDW amplitude (the green curve) corresponding to the intrawire junction in panel b. The red curve indicates the height profile along the black arrow in panel b. The inset shows the dI/dV curves measured at the points marked with vertical dashed lines in panel c.

meV. This corresponds to the minimum size of the band gap, being smaller than the gap estimated from centers of the spectral features for valence and conduction bands close to the Fermi energy. This value is consistent with the previous reports.[28−32] The gap is fully closed at the 4 × 1 side of the wire, where the STS spectrum shows finite conductance at the Fermi level (the blue curve). It is clearly shown in Figure 1c that the CDW gap, roughly the blue part, gradually decreases to completely collapse in the 4 × 1 part. The spatial distributions of the CDW gap (the black line) and the CDW

DOI: 10.1021/acs.nanolett.9b02438
Nano Lett. 2019, 19, 5769−5773

amplitude (green dots) obtained from the line STS map and the topographic height profile, respectively, show a direct quantitative correlation between electronic and atomic structures (Figure 1d). One may note the small deviation between both curves at the right-hand side of the junction (hatched with green lines). This discrepancy is not fundamental but instead is related to our own underestimation of the CDW gap mentioned above; as shown in the inset of Figure 1d, the STS spectral features growth further after the null conductance region has already shrunk to zero. In any case, the length of the intrawire electronic junction, defined from the change of the electronic structure, is about 7 ± 1 nm ($\sim 18a_0$).

In contrast, interwire interfaces between the two phases exhibit a sharply different behavior. In Figures 2a,b, the metallic and the CDW phases are connected perpendicular to the In wires. The boundary, imaged as a dark trench, is just a Si zigzag chain bonded to neighboring In chains. As is clear in the topographic contrast, the metallic phase is connected to the insulating phase abruptly. The spatial distribution of the CDW gap (Figure 2d) obtained from the dI/dV map clearly indicates the discrete jump of the gap size at the boundary. As a result, even a single metallic wire can be isolated as sandwiched between two 8 × 2 insulating domains (Figure 2b,c). Note that the CDW gap is fully collapsed even within a single-wire metallic domain. Thus, the CDW correlation length along this direction must be as small as 0.4 nm, just a single atomic unit cell. This result seems consistent with the anisotropy or the quasi-1D nature of the band structure.[28]

We further find that the electronic interface characterized above can be drastically affected by defects. Several well-defined atomic scale defects exist in addition to irregular vacancy and adatom clusters. One of the most well characterized and most popular among them is the so-called phase-flip defect,[31,33,34] which is also shown in Figure 3a. Its population increases linearly upon the increase of the In dose, indicating its atomic origin as excess In adsorbates. Our DFT calculations reveal the atomic structure of the excess In defect as shown Figure 4b (Figure S3 in Supporting Information). Figure 3a shows an STM image of an intrawire junction with

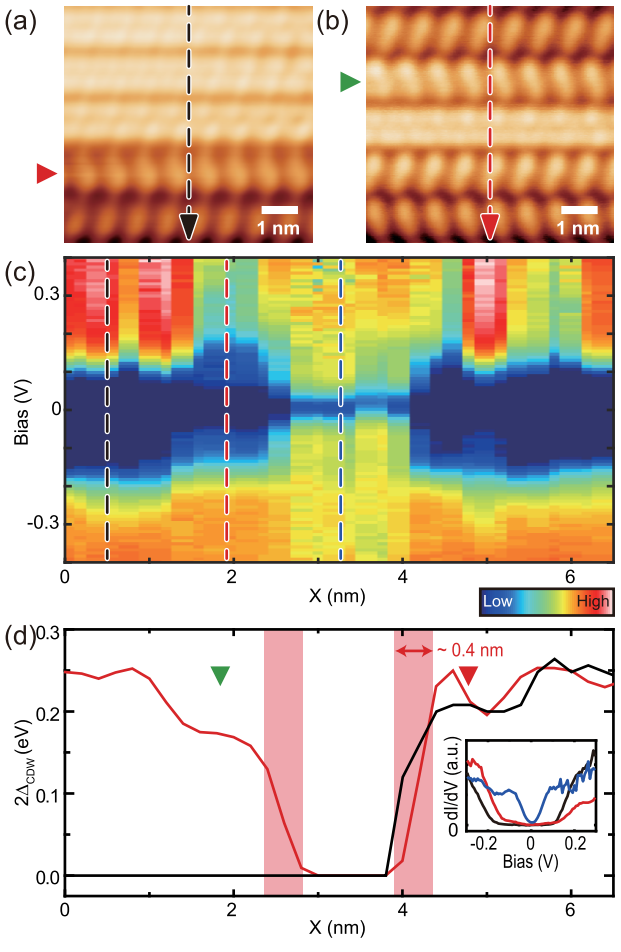

Figure 2. (a, b) STM images of the interwire junction between the 4 × 1 phase and the 8 × 2 phases taken at V_s = −0.5 V and I_t = 100 pA. (c) The spatially resolved dI/dV map (plotted in a logarithmic scale) taken along the red arrow in panel b. (d) The spatial distributions of the CDW gap in the dI/dV maps taken along the black and the red arrows in panels a and b, respectively. The inset shows the dI/dV curves measured at the points marked with vertical dashed lines in panel c.

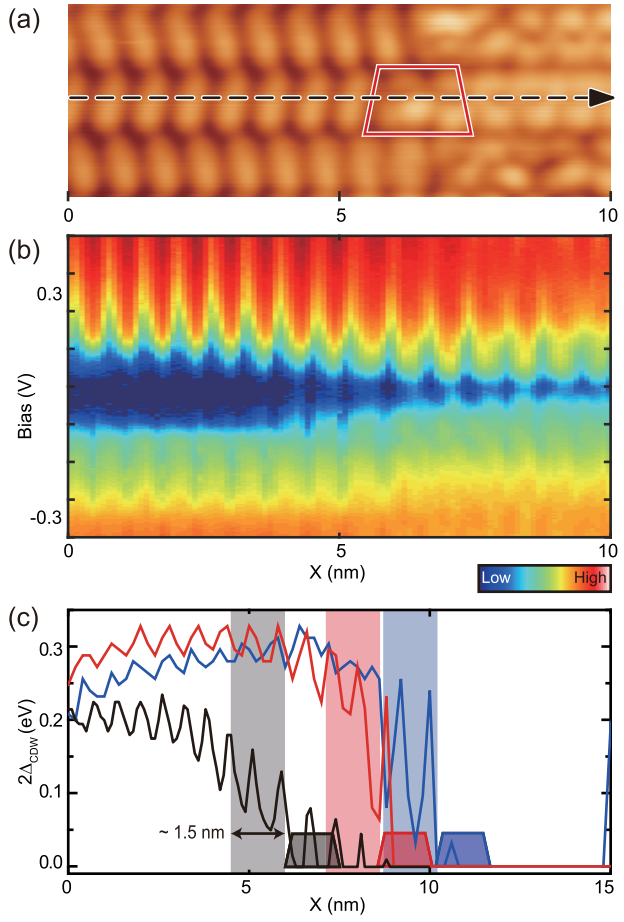

Figure 3. (a) STM image of the intrawire junction of the 4 × 1 phase and 8 × 2 phase with an atomic scale defect taken at V_s = −0.5 V and I_t = 100 pA. The red trapezoid indicates the atomic scale defect dividing two phases. (b) The spatially resolved dI/dV map (plotted in a logarithmic scale) taken along the black arrow in panel a. (c) The spatial distribution of the CDW gap size for three intrawire junctions with the same defect (Figure S2 in Supporting Information). The black curve corresponds to the dI/dV map of panel b. Each trapezoid indicates the position of the atomic scale defect corresponding to each curve, respectively. The vertical shade roughly indicates the region of the gap collapse toward each defect.

DOI: 10.1021/acs.nanolett.9b02438
Nano Lett. 2019, 19, 5769−5773

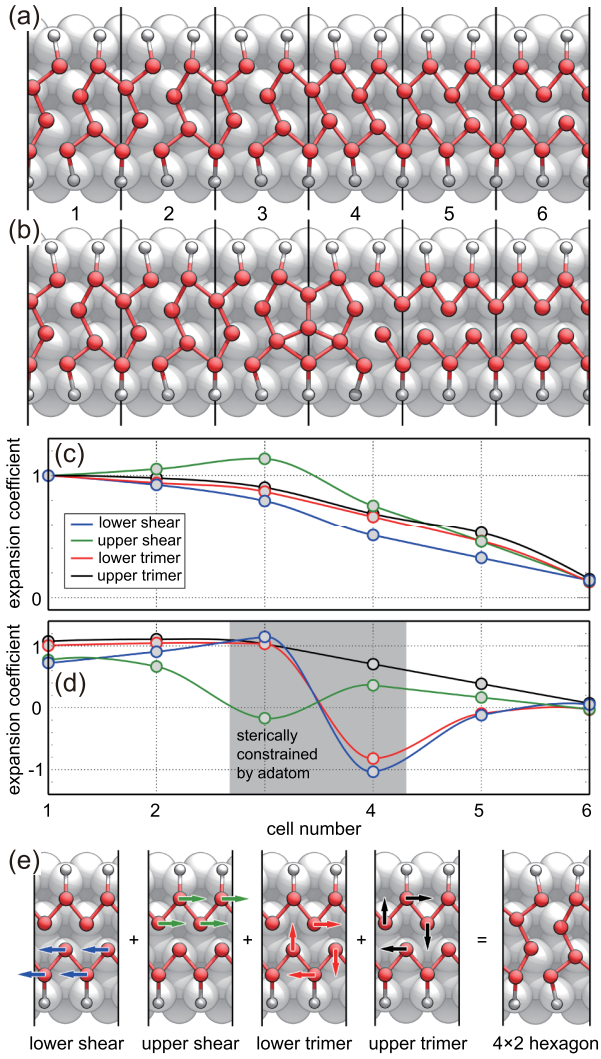

Figure 4. Schematic representation of (a) extended and (b) defect-induced abrupt intrawire junctions. Expansion of (c) extended and (d) abrupt junctions into configurational coordinates given by (e) the soft shear and rotary phonon eigenvectors that transform between the 4 × 1 and 8 × 2 phases, respectively. Data points are marked by circles, and solid lines provide a guide for the eye.

such a defect. In contrast to an intrinsic intrawire junction without a defect, the 8 × 2 and 4 × 1 phases are abruptly separated by this defect. The CDW oval structure of the 8 × 2 phase shows no significant change up to the very next unit cell to the defect. As straightforwardly expected from this topography, the spatially resolved dI/dV map obtained along this junction (Figure 3b) shows the abrupt change of the electronic state. While the gap size becomes uncertain very close to a defect, the CDW gap fully develops within only about 0.8−1.5 nm away from the edge of a defect in clear contrast to an intrinsic junction (Figure 3c). That is, the electronic junction length is reduced by an order of magnitude.

In order to understand the mechanism of the intrinsic and extrinsic junction formation, we performed DFT calculations. Counterintuitively, constructing a gradual transition from 4 × 1 to 8 × 2 analogous to Figure 1b as a static ground state structure turns out to be impossible. Intrinsic interfaces always relax into abrupt junctions between the 4 × 1 and 8 × 2 phases, even when using gradual structures as starting configurations. This is closely related to the first-order transition nature of the present system; the 4 × 1 and 8 × 2 phases both present local energy minima and any transition state is located somewhere on the energy barrier. We then performed first-principles molecular dynamics calculations to investigate the dynamical behavior for a $14a_0$ wire segment with its end points frozen in 8 × 2 and 4 × 1 configurations, respectively. After equilibration for 4 ps, we take an average of the structure over a trajectory length of 50 ps. For temperatures significantly below T_C, we observe moving phase fronts in accordance with ref 35. However, close to T_C, an equilibrium between both phases is reached and an extended intrawire junction on average is formed due to thermal fluctuations (Figure 4a). The simulated STM image for this dynamical interface is consistent with the experiment (Figure S4 in Supporting Information).

The mechanism by which defects reduce the junction length can then be traced to modifying or even suppressing these thermal fluctuations. We expand both the 4 × 1 and 4 × 2 (a simplified single-wire model of the 8 × 2 structure) structures into configurational coordinates given by the soft shear and rotary phonon eigenvectors that transform between the two phases (Figure 4e).[36,37] As shown in Figure 4c, for an extended junction, the configuration coordinates vary smoothly between 1 and 0, corresponding to the perfect 4 × 2 hexagon and 4 × 1 zigzag states, respectively. The presence of the defect, however, induces significant distortions to the wire that correspond to particular shear and trimerization states close to the defect (marked by the gray shade in Figure 4d). These configurations are sterically constrained by the defect, and thermal fluctuations can no longer visit the configurations associated with an extended intrawire junction. However, both the 4 × 2 and 4 × 1 structures are able to be interfaced with the In adatom defect with minimal strain that decays within a distance of a single a_0 as shown in Figure 4b. These results are consistent with the experimental observations. Note also that the abrupt interwire interface is related to the phonon modes too. The phonons involving the Si chains between In wires have much higher energies and are decoupled from the phonons of In wires, which prohibit the dynamical fluctuation across the wires under a finite interwire interaction.

In summary, we have investigated the atomic scale metal−insulator junctions formed on the electronically phase-separated In/Si(111) surface. The spatial distributions of the CDW gap and amplitude in various metal−insulator junctions indicate the strong anisotropy in the electronic junction lengths. The intrawire junction could be changed drastically by an atomic scale impurity to reduce the electronic junction length substantially. This result suggests a way of controlling electronic interfaces by impurity atoms or defects. The mechanism of the interface formation is revealed by calculations and simulations, where the dynamical nature of the interface is crucial. The strong coupling to specific phonon modes is the key physics underlying this mechanism and controllability. The physics and insight delivered in the present work can widely be applied in various electron−phonon-coupled systems where the separation and the switching of electronic phases are important.

■ ASSOCIATED CONTENT

Supporting Information

The Supporting Information is available free of charge on the ACS Publications website at DOI: 10.1021/acs.nanolett.9b02438.

DOI: 10.1021/acs.nanolett.9b02438
Nano Lett. 2019, 19, 5769−5773

Structure of the defect and the STM simulation of the dynamically extended junction (PDF)

AUTHOR INFORMATION

Corresponding Author

*E-mail: yeom@postech.ac.kr.

ORCID

Han Woong Yeom: 0000-0002-8538-8993

Author Contributions

S.K.S. performed the STM/STS measurements and analyzed the data. A.S. and S.W. performed the DFT calculations. S.K.S. and H.W. Y. wrote the manuscript with comments from the other authors. H.W.Y. supervised the research.

Notes

The authors declare no competing financial interest.

ACKNOWLEDGMENTS

S.K.S. and H.W.Y. were supported by Institute for Basic Science (IBS-R014-D1). S.W. gratefully acknowledges funding from the German Research Foundation (DFG) through FOR1700 and the German Ministry of Education and Research (BMBF) within the NanoMatFutur program (13N12972). The Max-Planck Computing and Data Facility, Garching, is acknowledged for providing supercomputer time.

REFERENCES

(1) Cheong, S.-W.; Sharma, P.; Hur, N.; Horibe, Y.; Chen, C. *Phys. B* **2002**, *318*, 39−51.

(2) Uehara, M.; Mori, S.; Chen, C. H.; Cheong, S.-W. *Nature* **1999**, *399*, 560−563.

(3) Park, J. T.; Inosov, D. S.; Niedermayer, C.; Sun, G. L.; Haug, D.; Christensen, N. B.; Dinnebier, R.; Boris, A. V.; Drew, A. J.; Schulz, L.; Shapoval, T.; Wolff, U.; Neu, V.; Yang, X.; Lin, C. T.; Keimer, B.; Hinkov, V. *Phys. Rev. Lett.* **2009**, *102*, 117006.

(4) de Mello, E.; Kasal, R.; Passos, C.; Filho, O. S. *Phys. B* **2009**, *404*, 3119−3122.

(5) Tao, J.; Niebieskikwiat, D.; Varela, M.; Luo, W.; Schofield, M. A.; Zhu, Y.; Salamon, M. B.; Zuo, J. M.; Pantelides, S. T.; Pennycook, S. J. *Phys. Rev. Lett.* **2009**, *103*, 097202.

(6) Du, K.; Zhang, K.; Dong, S.; Wei, W.; Shao, J.; Niu, J.; Chen, J.; Zhu, Y.; Lin, H.; Yin, X.; Liou, S.-H.; Yin, L.; Shen, J. *Nat. Commun.* **2015**, *6*, 6179.

(7) Zhu, Y.; Du, K.; Niu, J.; Lin, L.; Wei, W.; Liu, H.; Lin, H.; Zhang, K.; Yang, T.; Kou, Y.; Shao, J.; Gao, X.; Xu, X.; Wu, X.; Dong, S.; Yin, L.; Shen, J. *Nat. Commun.* **2016**, *7*, 11260.

(8) Lang, K. M.; Madhavan, V.; Hoffman, J. E.; Hudson, E. W.; Eisaki, H.; Uchida, S.; Davis, J. C. *Nature* **2002**, *415*, 412−416.

(9) Kinoda, G.; Hasegawa, T.; Nakao, S.; Hanaguri, T.; Kitazawa, K.; Shimizu, K.; Shimoyama, J.; Kishio, K. *Phys. Rev. B: Condens. Matter Mater. Phys.* **2003**, *67*, 224509.

(10) Morikawa, H.; Hwang, C. C.; Yeom, H. W. *Phys. Rev. B: Condens. Matter Mater. Phys.* **2010**, *81*, 075401.

(11) Zhang, H.; Ming, F.; Kim, H.-J.; Zhu, H.; Zhang, Q.; Weitering, H. H.; Xiao, X.; Zeng, C.; Cho, J.-H.; Zhang, Z. *Phys. Rev. Lett.* **2014**, *113*, 196802.

(12) Smith, N. V.; Kevan, S. D.; DiSalvo, F. J. *J. Phys. C: Solid State Phys.* **1985**, *18*, 3175.

(13) Coleman, R. V.; Drake, B.; Hansma, P. K.; Slough, G. *Phys. Rev. Lett.* **1985**, *55*, 394−397.

(14) Straub, T.; Finteis, T.; Claessen, R.; Steiner, P.; Hüfner, S.; Blaha, P.; Oglesby, C. S.; Bucher, E. *Phys. Rev. Lett.* **1999**, *82*, 4504−4507.

(15) Sipos, B.; Kusmartseva, A. F.; Akrap, A.; Berger, H.; Forró, L.; Tutiš, E. *Nat. Mater.* **2008**, *7*, 960.

(16) Cho, D.; Cheon, S.; Kim, K.-S.; Lee, S.-H.; Cho, Y.-H.; Cheong, S.-W.; Yeom, H. W. *Nat. Commun.* **2016**, *7*, 10453.

(17) Stojchevska, L.; Vaskivskyi, I.; Mertelj, T.; Kusar, P.; Svetin, D.; Brazovskii, S.; Mihailovic, D. *Science* **2014**, *344*, 177−180.

(18) Vaskivskyi, I.; Mihailovic, I. A.; Brazovskii, S.; Gospodaric, J.; Mertelj, T.; Svetin, D.; Sutar, P.; Mihailovic, D. *Nat. Commun.* **2016**, *7*, 1−6.

(19) Liu, G.; Debnath, B.; Pope, T. R.; Salguero, T. T.; Lake, R. K.; Balandin, A. A. *Nat. Nanotechnol.* **2016**, *11*, 845.

(20) Yoshida, M.; Suzuki, R.; Zhang, Y.; Nakano, M.; Iwasa, Y. *Science Advances* **2015**, *1*, e1500606.

(21) Yeom, H.; Takeda, S.; Rotenberg, E.; Matsuda, I.; Horikoshi, K.; Schaefer, J.; Lee, C.; Kevan, S.; Ohta, T.; Nagao, T.; Hasegawa, S. *Phys. Rev. Lett.* **1999**, *82*, 4898−4901.

(22) Kresse, G.; Furthmuller, J. *Comput. Mater. Sci.* **1996**, *6*, 15−50.

(23) Wippermann, S.; Schmidt, W. G. *Phys. Rev. Lett.* **2010**, *105*, 126102.

(24) Bunk, O.; Falkenberg, G.; Zeysing, J. H.; Lottermoser, L.; Johnson, R. L.; Nielsen, M.; Berg-Rasmussen, F.; Baker, J.; Feidenhans'l, R. *Phys. Rev. B: Condens. Matter Mater. Phys.* **1999**, *59*, 12228−12231.

(25) Gonzalez, C; Ortega, J; Flores, F *New J. Phys.* **2005**, *7*, 100.

(26) Shibasaki, T.; Nagamura, N.; Hirahara, T.; Okino, H.; Yamazaki, S.; Lee, W.; Shim, H.; Hobara, R.; Matsuda, I.; Lee, G.; Hasegawa, S. *Phys. Rev. B: Condens. Matter Mater. Phys.* **2010**, *81*, 035314.

(27) Yeom, H. W.; Oh, D. M.; Wippermann, S.; Schmidt, W. G. *ACS Nano* **2016**, *10*, 810−814.

(28) Ahn, J. R.; Byun, J. H.; Koh, H.; Rotenberg, E.; Kevan, S. D.; Yeom, H. W. *Phys. Rev. Lett.* **2004**, *93*, 106401.

(29) Park, S. J.; Yeom, H. W.; Min, S. H.; Park, D. H.; Lyo, I. W. *Phys. Rev. Lett.* **2004**, *93*, 106402.

(30) Tanikawa, T.; Matsuda, I.; Kanagawa, T.; Hasegawa, S. *Phys. Rev. Lett.* **2004**, *93*, 016801.

(31) Zhang, H.; Choi, J.-H.; Xu, Y.; Wang, X.; Zhai, X.; Wang, B.; Zeng, C.; Cho, J.-H.; Zhang, Z.; Hou, J. G. *Phys. Rev. Lett.* **2011**, *106*, 026801.

(32) Uetake, T.; Hirahara, T.; Ueda, Y.; Nagamura, N.; Hobara, R.; Hasegawa, S. *Phys. Rev. B: Condens. Matter Mater. Phys.* **2012**, *86*, 035325.

(33) Kim, T. H.; Yeom, H. W. *Phys. Rev. Lett.* **2012**, *109*, 1−5.

(34) Cheon, S.; Kim, T.-H.; Lee, S.-H.; Yeom, H. W. *Science* **2015**, *350*, 182−185.

(35) Wall, S.; Krenzer, B.; Wippermann, S.; Sanna, S.; Klasing, F.; Hanisch-Blicharski, A.; Kammler, M.; Schmidt, W. G.; Horn-von Hoegen, M. *Phys. Rev. Lett.* **2012**, *109*, 186101.

(36) Schmidt, W. G.; Wippermann, S.; Sanna, S.; Babilon, M.; Vollmers, N. J.; Gerstmann, U. *Phys. Status Solidi B* **2012**, *249*, 343−359.

(37) Speiser, E.; Esser, N.; Wippermann, S.; Schmidt, W. G. *Phys. Rev. B: Condens. Matter Mater. Phys.* **2016**, *94*, 075417.

DOI: 10.1021/acs.nanolett.9b02438
Nano Lett. 2019, 19, 5769−5773